Antibody responses to SARS-CoV-2 variants LP.8.1, LF.7.1, NB.1.8.1, XFG and BA.3.2 following KP.2 monovalent mRNA vaccination

Anass Abbad[a,b], Brian Lerman[a,b], Jordan Ehrenhaus[a,b], Brian Monahan[a,b], Gagandeep Singh[a,b], Adria Wilson[a,b], Stefan Slamanig[a], Ashley Aracena[a,b], Neko Lyttle[a,b], Jessica Nardulli[a,b], Keith Farrugia[c], Zain Khalil[c], Ana Silvia Gonzalez-Reiche[c], Mia Emilia Sordillo[d], Weina Sun[a], Harm van Bakel[c], Viviana Simon[a,b,c,d,e], Florian Krammer[a,b,d,f,g]

Affiliations:

[a] Department of Microbiology, Icahn School of Medicine at Mount Sinai, New York, USA

[b] Center for Vaccine Research and Pandemic Preparedness (C-VaRPP), Icahn School of Medicine at Mount Sinai, New York, USA

[c] Department of Genetics and Genomic Sciences, Icahn School of Medicine at Mount Sinai, New York, USA.

[d] The Global Health and Emerging Pathogens Institute, Icahn School of Medicine at Mount Sinai, New York, USA

[e] Department of Pathology, Molecular and Cell Based Medicine, Icahn School of Medicine at Mount Sinai, New York, USA

[f] Division of Infectious Diseases, Department of Medicine, Icahn School of Medicine at Mount Sinai, New York, USA

[g] Ignaz Semmelweis Institute, Interuniversity Institute for Infection Research, Medical University of Vienna, Vienna, Austria

[h] Ludwig Boltzmann Institute for Science Communication and Pandemic Preparedness at the Medical University of Vienna, Medical University of Vienna, Vienna, Austria

Correspondence to: Prof Florian Krammer and Prof. Viviana Simon, Department of Microbiology, Icahn School of Medicine at Mount Sinai, 1 Gustave L Levy Place, New York, NY 10029, USA. florian.krammer@mssm.edu

Word count: 759 words

Summary word count: 141 words

In brief word count: 69 words

Summary

The evolution of SARS-CoV-2 has resulted in antigenically distinct variants that challenge vaccine-induced immunity. The KP.2 monovalent mRNA vaccine was deployed in 2024 to address immune escape by emerging SARS-CoV-2 subvariants. We assessed neutralizing antibody responses in 56 adults with varied exposure histories following KP.2 vaccination against emerging variants including LP.8.1, LF.7.1, NB.1.8.1, XFG, and BA.3.2. While KP.2 vaccination enhanced neutralization against homologous variants, dramatic reductions in neutralizing activity were observed against FLiRT variants across all exposure groups. Critically, exposure history profoundly influenced neutralization breadth, with vaccination-only participants exhibiting superior cross-neutralization compared to individuals with hybrid immunity. Antigenic cartography revealed substantial antigenic distances between KP.2 and emerging variants, highlighting significant immune escape potential that threatens vaccine protection. Overall, our data suggest that KP.2 boosting predominantly enhances cross-reactive responses imprinted by previously encountered spike antigens, with limited adaptation to antigenically drifted variants.

In Brief

SARS-CoV-2 continues to evolve, producing variants that escape vaccine-induced immunity. Abbad et al. show that KP.2 monovalent vaccination provides limited protection against antigenically distant FLiRT variants (LP.8.1, LF.7.1, NB.1.8.1, XFG) and BA.3.2. Surprisingly, vaccination-only individuals exhibited broader cross-neutralizing responses than those with hybrid immunity, suggesting that infection history may narrow antibody responses through immune imprinting. These findings highlight the ongoing challenge of maintaining vaccine effectiveness against evolving SARS-CoV-2 variants.

Highlights

- KP.2 vaccination shows reduced neutralization against emerging variant strains
- Vaccination-only individuals exhibit broader responses
- Recent infections before vaccination create bias toward ancestral strain
- Binding antibodies remain strong despite poor neutralization of new variants
- Antigenic mapping show major antigenic distances between KP.2 and emerging variants

Introduction

SARS-CoV-2 continues evolving in immunologically experienced populations, with emerging variants demonstrating enhanced immune escape capabilities. The KP.2 monovalent mRNA vaccine was deployed in 2024 and may still be employed during the 2025/26 winter season.[1] However, the impact of diverse exposure histories on cross-protection against antigenically distant variants remains poorly characterized. Understanding neutralizing antibody responses against emerging variants is crucial for informing vaccine strategy and pandemic preparedness. Here, we assessed neutralizing and binding antibody responses in 56 adult study participants with varied SARS-CoV-2 exposure histories following KP.2 monovalent vaccination.

Results

Study Design and Participants

We enrolled 56 healthy adults who received KP.2 monovalent mRNA vaccines and stratified them by exposure profile: vaccination-only (n=16, self-reported, with no strong evidence of any past infection), post-infection boosted (n=11, booster vaccination soon after an infection), and complex hybrid immunity (n=29, ≥2 infections plus ≥3 vaccine doses) (Table 1). Serum samples were collected an average of 29 days post-vaccination. We measured neutralizing antibodies against ancestral WA.1, vaccine-matched KP.2, JN.1 and emerging variants including LP.8.1, LF.7.1, NB.1.8.1, XFG, and BA.3.2 using live and pseudotyped virus microneutralization assays. The tested variants harbor distinct mutation patterns in key antigenic sites (Figure 1A). BA.3.2, a saltation variant with >50 mutations relative to BA.3, was originally identified in South Africa but has subsequently been detected globally (e.g. Germany, the Netherlands, California, and Australia), reflecting its capacity for transmission despite antigenic divergence.[2,3] FLiRT variants contain critical mutations including R346T, F456L, and Q498R that enhance both ACE2 binding and antibody evasion.

Table 1. Demographics, SARS-CoV-2 infection and vaccination summary table of post-KP.2 boosted cohort. Summary information for a total of 56 individuals collected serum samples (average of 29 days) following mRNA monovalent KP.2 vaccine booster.

		Vaccination Only	Post-Infection Boosted	Complex Hybrid Immunity	Total
N total		16	11	29	56
Age		avg (min – max)	avg (min – max)	avg (min – max)	avg (min – max)
		44.8 (20 – 75)	40.5 (25 – 62)	41.4 (23 – 81)	42.2 (20 – 81)
Sex at Birth		n (% group)	n (% group)	n (% group)	n (% total)
	Female	11 (68.75%)	8 (72.73%)	23 (79.31%)	42 (75%)
	Male	5 (31.25%)	3 (27.27%)	6 (20.69%)	14 (25%)
Bivalent Boost		n (% group)	n (% group)	n (% group)	n (% total)
	Yes	11 (68.75%)	10 (90.91%)	19 (65.52%)	40 (71.43%)

No	5 (31.25%)	1 (9.09%)	10 (34.48%)	16 (28.57%)
XBB Boost	n (% group)	n (% group)	n (% group)	n (% total)
Yes	9 (56.25%)	6 (54.55%)	24 (82.76%)	39 (69.64%)
No	7 (43.75%)	5 (45.45%)	5 (17.24%)	17 (30.36%)
Infection	n (% group)	n (% group)	n (% group)	n (% total)
Yes	0 (0%)	11 (100%)	29 (100%)	42 (75%)
No	16 (100%)	0 (0%)	0 (0%)	14 (25%)
KP.2 vaccination type	n (% group)	n (% group)	n (% group)	n (% total)
Pfizer	12 (75%)	4 (36.36%)	19 (65.52%)	35 (62.5%)
Moderna	4 (25%)	7 (63.64%)	10 (34.48%)	21 (37.5%)

91

92

Neutralizing and Binding Antibody Responses

KP.2 vaccination enhanced neutralization against homologous KP.2 (GMT: 315) and closely related JN.1 (GMT: 203) variants (Figure 1B-E). However, post-KP.2 vaccine sera showed dramatically reduced neutralization against FLiRT variants across all exposure groups. Neutralizing titers against WA.1 (GMT: 733) significantly exceeded those against LP.8.1 (GMT: 60, $p<0.0001$), LF.7.1 (GMT: 92, $p<0.0001$), NB.1.8.1 (GMT: 40, $p<0.0001$), and XFG (GMT: 29, $p<0.0001$). BA.3.2 showed intermediate neutralization (GMT: 197), representing a 3-fold reduction compared to ancestral strain.

Critically, exposure history profoundly influenced neutralization breadth (Figure 1F). Participants with vaccination-only immunity exhibited the most potent and broad responses, with highest titers against KP.2 (GMT: 461), JN.1 (GMT: 298), and superior neutralization of FLiRT variants compared to other groups (Figure 1C). Conversely, post-infection boosted participants exhibited the strongest ancestral bias (WA.1 GMT: 874) and weakest cross-neutralization: LP.8.1 (GMT: 39), LF.7.1 (GMT: 76), NB.1.8.1 (GMT: 29), and XFG (GMT: 17) (Figure 1E). Participants with complex hybrid immunity showed intermediate patterns across all variants (Figure 1D).

Antigenic cartography quantified these escape patterns [4,5], revealing that emerging variants occupy distant positions in antigenic space relative to KP.2 (Figure 1G). FLiRT variants clustered at antigenic distances exceeding three units from KP.2 (representing >8-fold neutralization reductions), while BA.3.2 occupied an intermediate but distinctly separate position. This spatial organization directly correlates with neutralization data and shows substantial immune escape potential that threatens protection.

Despite poor neutralization, binding antibody responses remained robust across all groups (Figure 2), with binding-to-neutralizing ratios progressively increasing for divergent variants (Figure 3), particularly in individuals with hybrid immunity. This preservation of binding capacity suggests maintained protection against severe disease.[6,7]

Discussion

Our findings reveal significant challenges posed by continued SARS-CoV-2 antigenic evolution. The dramatic reduction in neutralizing activity against FLiRT variants, driven by mutations in critical antigenic sites, highlights the enhanced immune escape capabilities of these variants. The unexpected finding that vaccination-only participants showed superior cross-neutralization compared to individuals with hybrid immunity challenges conventional assumptions about hybrid immunity advantages.

The intermediate neutralization reduction observed for BA.3.2, despite its extensive mutation profile. While unlikely, this could be an artifact of the pseudotype virus system used. However, it may explain why this variant has not achieved high transmission rates globally. This could reflect a balance between immune escape and viral fitness costs associated with extensive mutations.

These data highlight the need for adaptive vaccine approaches. Future strategies should consider targeting conserved epitopes or employing alternative delivery methods such as intranasal vaccination to enhance mucosal protection.[8] Continuous antigenic surveillance and rapid vaccine updates will be essential as SARS-CoV-2 continues evolving in immunologically experienced populations.

Limitations of the study

This study has several limitations. The sample size, while adequate for detecting major differences, may limit detection of subtle variations between subgroups. The pseudotype system used for BA.3.2 testing may not fully recapitulate live virus neutralization. Additionally, the durability of these responses beyond the measured timepoint remains unknown. Here, only serological responses were evaluated; cellular immunity, which significantly contributes to protection, was not assessed. Despite these limitations, the observed trends in immune escape and antibody quality remain relevant for informing ongoing vaccine updates and public health strategies.

Acknowledgements

This study would not have been feasible without the sustained assistance of the generous research participants, and we thank them for their contribution. We are also thankful to the Mount Sinai Pathogen Surveillance Program for providing representative Omicron viral isolates in a timely manner.

This study was supported by the NIAID Centers of Excellence for Influenza Research and Response (CEIRR, 75N93021C00014, FK and VS), the NIAID Collaborative Influenza Vaccine Innovation Centers (CIVIC, 75N39019C00051, FK and VS) and institutional funding. This project has been funded in part with Federal funds from the National Cancer Institute, National Institutes of Health, under Contract No. 75N91019D00024, Task Order No. 75N91021F00001. The content of this publication does not necessarily reflect the views or policies of the Department of Health and Human Services, nor does mention of trade names, commercial products or organizations imply endorsement by the U.S. Government.

The Conventional Biocontainment Facility (CBF) is a NIHBSL3/BSL3 facility that is part of the BSL-3 Biocontainment CoRE. This Core is supported by subsidies from the ISMMS Dean's Office and by investigator support through a cost recovery mechanism. Research reported in this publication was supported by the National Institute of Allergy and Infectious Diseases of the National Institutes of Health under Award Number G20AI174733 (R.A. Albrecht). The content is solely the responsibility of the authors and does not necessarily represent the official views of the National Institutes of Health.

Declaration of interests

FK declares the following conflicts of interest. The Icahn School of Medicine at Mount Sinai has filed patent applications regarding influenza virus vaccines on which FK is listed as inventor. The Icahn School of Medicine at Mount Sinai has filed patent applications relating to SARS-CoV-2 serological assays, NDV-based SARS-CoV-2 vaccines, influenza virus vaccines and influenza

virus therapeutics which list FK as co-inventor. Dr. Simon is also listed on the SARS-CoV-2 serological assays patent.

FK has received royalty payments from some of these patents. Mount Sinai has spun out a company, Castlevax, to develop SARS-CoV-2 vaccines. FK is co-founder and scientific advisory board member of Castlevax. FK has consulted for Merck, GSK, Sanofi, Curevac, Gritstone, Seqirus and Pfizer and is currently consulting for 3rd Rock Ventures and Avimex. The Krammer laboratory is also collaborating with Dynavax on influenza vaccine development. The Simon and van Bakel labs collaborate with Sanofi Pasteur on pathogen surveillance.

Author Contributions

AA, BL, JE, AW and GS conducted experiments. AA, BL and BM contributed to data analysis. BM and KS assisted with sample processing and data collection. SS and WS shared rcVSV-spike pseudoviruses. FK and VS conceived and supervised the study, designed experiments, analyzed data. AA, VS and FK wrote the manuscript. All authors reviewed and approved the final manuscript.

Figure legend

Figure 1: Neutralizing antibody responses and antigenic relationships following KP.2 vaccination. (A) Functional classification of SARS-CoV-2 spike mutations across major variants. Heatmap displaying amino acid mutations in the SARS-CoV-2 spike protein across eight major variants (WA.1, JN.1, KP.2, LP.8.1, LF.7.1, NB.1.8.1, XFG, and BA.3.2) colored by predicted functional impact on receptor binding, antibody escape, and structural stability. Variants are organized by evolutionary lineage, with spike protein domains (N-terminal domain, receptor-binding domain, S1 and S2) indicated. Dendrogram illustrate antigenic similarity relationships based on mutation patterns, with variants clustering by phylogenetic relationship. Color intensity reflects the magnitude of predicted functional consequences for each substitution. **(B) Neutralizing antibody titers following KP.2 monovalent vaccination across exposure groups** against the variant panel for the overall cohort, **(C)** vaccination-only group, **(D)** complex hybrid immunity group and **(E)** recent infection hybrid group. **(F)** Comparative GMT trends across all exposure groups overlaid on a single graph, showing neutralization patterns against each tested variant. Dashed lines connect GMT values for each group. Data are presented as aligned dot plots with individual participant responses connected by lines across the tested virus panel, allowing visualization of individual neutralization patterns. Statistical comparisons between variants within each exposure group are shown above brackets, with significance determined by one-way ANOVA with Dunnett's multiple comparisons test. (G) **Antigenic cartography reveals spatial relationships between SARS-CoV-2 variants.** Two-dimensional antigenic map constructed from neutralizing antibody titers of the overall KP.2-boosted cohort against the tested variant panel. Each circle represents a virus variant, and each square a unique serum biospecimen, with distances proportional to antigenic differences based on neutralization data. Closely related variants cluster together, while antigenically distinct variants occupy distant positions. Grid lines represent 2-fold changes in neutralizing antibody titers, with each unit corresponding to a 2-fold difference. The

map illustrates the antigenic landscape surrounding KP.2, highlighting the substantial antigenic drift of FLiRT variants (LP.8.1, LF.7.1, NB.1.8.1, XFG) and the intermediate positioning of BA.3.2 relative to the vaccine and ancestral strains.

Figure 2. Binding antibody responses to SARS-CoV-2 spike proteins following KP.2 vaccination. (A-D) Binding antibody area under the curve (AUC) titers against wild-type (WT) and JN.1 spike proteins for the overall cohort (A), vaccination-only group (B), complex hybrid immunity group (C) and recent infection hybrid group (D). Data are presented as aligned dot plots with individual participant binding responses connected by lines between WT and JN.1 spike antigens, demonstrating paired serological profiles for each individual. Statistical significance for paired comparisons is determined by Wilcoxon matched-pairs signed rank test.

Figure 3. Binding-to-neutralizing antibody ratios reveal functional antibody quality across variants. (A-D) Ratios of wild-type spike binding AUC to neutralizing ID50 titers for each tested variant in the overall cohort (A), vaccination-only group (B), complex hybrid immunity group (C) and recent infection hybrid group (D). (E-H) Ratios of JN.1 spike binding AUC to neutralizing ID50 titers across the same groupings. Data are presented as scatter plots with individual participant ratios plotted for each variant. Geometric mean ratios (GMR) are indicated by horizontal lines with standard deviation error bars. Higher ratios indicate preserved binding capacity with reduced neutralizing efficiency. Statistical comparisons between variants within each exposure group are shown above brackets, with significance determined by one-way ANOVA with Dunnett's multiple comparisons test.

References

1. Link-Gelles, R., Chickery, S., Webber, A., Ong, T.C., Rowley, E.A.K., DeSilva, M.B., Dascomb, K., Irving, S.A., Klein, N.P., Grannis, S.J., et al. (2025). Interim Estimates of 2024-2025 COVID-19 Vaccine Effectiveness Among Adults Aged >/=18 Years - VISION and IVY Networks, September 2024-January 2025. MMWR Morb Mortal Wkly Rep *74*, 73-82. 10.15585/mmwr.mm7406a1.
2. Zhang, L., Kempf, A., Nehlmeier, I., Chen, N., Stankov, M.V., Happle, C., Dopfer-Jablonka, A., Behrens, G.M.N., Schulz, S.R., Jack, H.M., et al. (2025). Host cell entry and neutralisation sensitivity of SARS-CoV-2 BA.3.2. Lancet Microbe, 101165. 10.1016/j.lanmic.2025.101165.
3. Guo, C., Yu, Y., Liu, J., Jian, F., Yang, S., Song, W., Yu, L., Shao, F., and Cao, Y. (2025). Antigenic and virological characteristics of SARS-CoV-2 variants BA.3.2, XFG, and NB.1.8.1. Lancet Infect Dis *25*, e374-e377. 10.1016/S1473-3099(25)00308-1.
4. Wilks, S.H., Muhlemann, B., Shen, X., Tureli, S., LeGresley, E.B., Netzl, A., Caniza, M.A., Chacaltana-Huarcaya, J.N., Corman, V.M., Daniell, X., et al. (2023). Mapping SARS-CoV-2 antigenic relationships and serological responses. Science *382*, eadj0070. 10.1126/science.adj0070.
5. Smith, D.J., Lapedes, A.S., de Jong, J.C., Bestebroer, T.M., Rimmelzwaan, G.F., Osterhaus, A.D., and Fouchier, R.A. (2004). Mapping the antigenic and genetic evolution of influenza virus. Science *305*, 371-376. 10.1126/science.1097211.
6. Clark, J.J., Hoxie, I., Adelsberg, D.C., Sapse, I.A., Andreata-Santos, R., Yong, J.S., Amanat, F., Tcheou, J., Raskin, A., Singh, G., et al. (2024). Protective effect and molecular mechanisms of human non-neutralizing cross-reactive spike antibodies elicited by SARS-CoV-2 mRNA vaccination. Cell Rep *43*, 114922. 10.1016/j.celrep.2024.114922.
7. Vikstrom, L., Fjallstrom, P., Gwon, Y.D., Sheward, D.J., Wigren-Bystrom, J., Evander, M., Bladh, O., Widerstrom, M., Molnar, C., Rasmussen, G., et al. (2023). Vaccine-induced correlate of protection against fatal COVID-19 in older and frail adults during waves of neutralization-resistant variants of concern: an observational study. Lancet Reg Health Eur *30*, 100646. 10.1016/j.lanepe.2023.100646.
8. Slamanig, S., Gonzalez-Dominguez, I., Chang, L.A., Lemus, N., Lai, T.Y., Martinez, J.L., Singh, G., Dolange, V., Abdeljawad, A., Kowdle, S., et al. (2024). Intranasal SARS-CoV-2 Omicron variant vaccines elicit humoral and cellular mucosal immunity in female mice. EBioMedicine *105*, 105185. 10.1016/j.ebiom.2024.105185.

1 **STAR METHODS**

2 **Key resources table**

REAGENT or RESOURCE	SOURCE	IDENTIFIER
Antibodies		
Anti-human IgG (Fab-specific) horseradish peroxidase antibody	Sigma-Aldrich	Cat#A0293, RRID: AB_257875
Mouse anti-SARS nucleoprotein monoclonal antibody (1C7C7)	Center for Therapeutic Antibody Development at the Icahn School of Medicine at Mount Sinai	N/A
Bacterial and virus strains		
SARS-CoV-2 isolate USA-WA1/2020 strain	BEI Resources	NR52281
SARS-CoV-2 isolate JN.1 (hCoV-19/USA/NY-MSHSPSP-PV96109/2023)	Simon and Krammer laboratory at the Icahn School of Medicine at Mount Sinai	Reagents | Krammer Laboratory (mssm.edu)
SARS-CoV-2 isolate KP.2 (hCoV-19/USA/NY-MSHSPSP-PV112116/2024)	Simon and Krammer laboratory at the Icahn School of Medicine at Mount Sinai	Reagents | Krammer Laboratory (mssm.edu)
SARS-CoV-2 isolate LF.7.1 (hCoV-19/USA/NY-MSHSPSP-PV301501/2025)	Simon and Krammer laboratory at the Icahn School of Medicine at Mount Sinai	Reagents | Krammer Laboratory (mssm.edu)
SARS-CoV-2 isolate LP.8.1 (hCoV-19/USA/NY-MSHSPSP-PV301922/2024)	Simon and Krammer laboratory at the Icahn School of Medicine at Mount Sinai	Reagents | Krammer Laboratory (mssm.edu)
SARS-CoV-2 isolate NB.1.8.1 (hCoV-19/USA/NY-MSHSPSP-PV304487/2025)	Simon and Krammer laboratory at the Icahn School of Medicine at Mount Sinai	Reagents | Krammer Laboratory (mssm.edu)
SARS-CoV-2 isolate XFG (hCoV-19/USA/NY-MSHSPSP-PV304164/2025)	Simon and Krammer laboratory at the Icahn School of Medicine at Mount Sinai	Reagents | Krammer Laboratory (mssm.edu)
rcVSV-eGFP-CoV2-S (USA-WA1/2020 strain)	Simon and Krammer laboratory at the Icahn School of Medicine at Mount Sinai	Reagents | Krammer Laboratory (mssm.edu)
rcVSV-eGFP-CoV2-S BA.3.2 (hCoV-19/South Africa/NICD-R00178/2025)	Simon and Krammer laboratory at the Icahn School of Medicine at Mount Sinai	Reagents | Krammer Laboratory (mssm.edu)
Biological samples		
Human serum samples from healthcare workers	Simon laboratory at the Icahn School of Medicine at Mount Sinai	https://labs.icahn.mssm.edu/simonlab/
Chemicals, peptides, and recombinant proteins		
Recombinant spike (S)	Krammer laboratory at the Icahn School of Medicine at Mount Sinai	https://labs.icahn.mssm.edu/ krammerlab/reagents/

SIGMAFAST ™ OPD (*o*-phenylenediamine dihydrochloride)	Sigma-Aldrich	Cat# P9187
3M hydrochloric acid	Thermo Fisher Scientific	Cat# S25856
Tween20	Fisher Bioreagents	Cat# BP337-100
Non-Fat Dry Milk Omniblok	AmericanBio	Cat# AB10109-01000
Experimental models: Cell lines		
African green monkey Vero-E6 cells expressing Transmembrane protease serine2 (TMPRSS2)	BPSBiosciences	Cat#78081
Expi293F cells	Gibco	Cat#A14527
Baby hamster kidney cells expressing angiotensin converting enzyme 2 (BHK-ACE2)	Weina laboratory at the Icahn School of Medicine at Mount Sinai	Not applicable
Recombinant DNA		
pCAGGS	https://www.ncbi.nlm.nih.gov/pmc/articles/PMC4248980/	Not applicable
pCAGGS SARS-CoV-2 WT spike	Krammer laboratory at the Icahn School of Medicine at Mount Sinai	Not applicable
pCAGGS SARS-CoV-2 JN.1 spike	Krammer laboratory at the Icahn School of Medicine at Mount Sinai	Not applicable
Software and algorithms		
Prism 10	GraphPad	https://www.graphpad.com
R studio (R version 4.3.3)	The Comprehensive R Archive Network (CRAN)	https://github.com/kalibera/ucrt3
Racmacs (version 1.2.9)	Racmacs	https://acorg.github.io/Racmacs/
ComplexHeatmap (version 2.22.0)	The Comprehensive R Archive Network (CRAN)	https://doi.org/doi:10.18129/B9.bioc.ComplexHeatmap

RESOURCE AVAILABILITY

Lead contact

information and requests for resources and reagents should be directed to and will be fulfilled by the lead contact, Florian Krammer (florian.krammer@mssm.edu).

Materials availability

Unique reagents used in the study are available upon request from the lead author.

Data and code availability

- All data will be available from ImmPort under the following identifier: SDYxxxx. No code was used or developed for this study.
- Any additional information required to reanalyze the data reported in this paper is available from the lead contact upon request.

EXPERIMENTAL MODEL AND STUDY PARTICIPANT DETAILS

Human cohort description

De-identified human serum samples were collected from 56 healthy participants enrolled in the following observational studies: PARIS (Protection Associated with Rapid Immunity to SARS-CoV-2, IRB20-03374) and the observational longitudinal clinical sample collection from patients with emerging viral infections (IRB-17-00791/STUDY-16-01215) at the Icahn School of Medicine at Mount Sinai. All participants received KP.2 monovalent mRNA vaccines and were stratified based on their SARS-CoV-2 exposure history. These studies were approved by the Mount Sinai Hospital Institutional Review Board and all participants provided written informed consent prior to sample and data collection. Information regarding COVID-19 vaccination, SARS-CoV-2 infection were participant reported. Demographics and immune history analysis are shown in Table 1.

Cell culture

Vero-E6 cells expressing transmembrane protease serine 2 (TMPRSS2) (BPS Biosciences, cat. no. 78081) were maintained in Dulbecco's modified Eagle's medium (DMEM; Gibco, cat. no. 11965092) supplemented with 10% heat-inactivated fetal bovine serum (FBS; Gibco, cat. no. A5256801), 1% minimum essential medium with non-essential amino acids (Gibco, cat. no. 11140050), 100 U/mL penicillin and 100 µg/mL streptomycin (Gibco, cat. no. 15140122), 100 µg/mL normocin (InvivoGen, cat. no. ant-nr), and 3 µg/mL puromycin (InvivoGen, cat. no. ant-pr). Baby hamster kidney cells expressing angiotensin converting enzyme 2 (BHK-ACE2) cells were cultured in DMEM supplemented with 10% FBS and 1% penicillin/streptomycin. Expi293F cells (Gibco, cat. no. A14527) were maintained in Expi293 Expression Medium (Gibco, cat. no. A1435102).

Replication competent SARS-CoV-2 isolates

The SARS-CoV-2 isolate USA-WA.1/2020 was used as a wild-type/ancestral reference (BEI Resources; NR-52281). The following viral isolates from the Omicron lineage were provided by the Mount Sinai Pathogen Surveillance Program: hCoV-19/USA/NY-MSHSPSP-PV96109/2023 (JN.1), hCoV-19/USA/NY-MSHSPSP-PV112116/2024 (KP.2), hCoV-19/USA/NY-MSHSPSP-PV301922/2024 (LP.8.1), hCoV-19/USA/NY-MSHSPSP-PV301501/2025 (LF.7.1), hCoV-19/USA/NY-MSHSPSP-PV304487/2025 (NB.1.8.1), and hCoV-19/USA/NY-MSHSPSP-PV304164/2025 (XFG).

Recombinant protein production

SARS-CoV-2 spike ectodomain proteins were produced using mammalian expression systems as previously described [1]. Codon-optimized sequences encoding spike proteins from wild-type (WT; ancestral Wuhan-Hu-1, GenBank: MN908947) and JN.1 variant strains (GenBank: PP298019) were cloned into pCAGGs expression vectors. Recombinant proteins were expressed in Expi293F cells using the ExpiFectamine 293 Transfection Kit (Thermo Fisher Scientific). Cell culture supernatants were harvested 72 hours post-transfection, clarified by centrifugation at 4,000 × g, filtered, and purified using Ni^{2+}-nitrilotriacetic acid (Ni-NTA) agarose (Qiagen, cat. no. 30210). Purified proteins were concentrated using Amicon Ultracell centrifugal units (EMD Millipore, cat. no. C7715), buffer-exchanged to phosphate-buffered saline (1× PBS, pH 7.4), verified by sodium dodecyl sulfate polyacrylamide gel electrophoresis (SDS-PAGE), and stored at −80°C until use.

Enzyme-linked immunosorbent assay (ELISA)

IgG binding antibody titers against SARS-CoV-2 WT and JN.1 spike proteins were measured using an in-house ELISA. Briefly, 96-well microtiter plates (Immulon 4 HBX; Thermo Scientific, cat. no. 439454) were coated overnight at 4°C with 2 µg/mL recombinant spike protein. After washing with 1× phosphate buffered saline supplement with 0.1 % Tween 20 (PBS-T) and blocking with 3% milk powder in PBS-T for 1 hour at room temperature, heat-inactivated sera were added in 2-fold serial dilutions starting at 1:100. Following 2-hour incubation and washing, anti-human IgG (Fab-specific) horseradish peroxidase (HRP)-conjugated secondary antibody (Sigma-Aldrich, cat. no. A0293) was added at 1:3,000 dilution. After 1-hour incubation and washing, o-phenylenediamine dihydrochloride substrate (SIGMAFAST) was added for 10 minutes, and the reaction was stopped with 3 M HCl. Optical density was measured at 490 nm using a Synergy H1 microplate reader (BioTek), and area under the curve (AUC) values were calculated using Prism 10 (GraphPad).

Replication competent SARS-CoV-2 neutralization assay

Neutralizing antibody titers against SARS-CoV-2 variants (WA.1, JN.1, KP.2, LP.8.1, LF.7.1, NB.1.8.1, and XFG) were measured using a multicycle microneutralization assay in a BSL-3 facility. Vero-E6 TMPRSS2 cells (2×10^5 cells/well) were seeded in 96-well plates 24 hours prior to infection. Heat-inactivated sera were 3-fold serially diluted starting at 1:10 in modified Eagle's medium (1xMEM) and incubated with 10,000 50% tissue culture infectious dose ($TCID_{50}$) of each virus for 1 hour at room temperature. Virus-serum mixtures were transferred to cell plates and incubated for 1 hour at 37°C. After removing inoculum, 1xMEM supplemented with 2% FBS was added, and plates were incubated for 48 hours at 37°C. Cells were fixed with 10% formaldehyde overnight at 4°C, permeabilized with 0.1% Triton X-100, and blocked with 3% bovine serum albumin (BSA) in PBS. Biotinylated anti-SARS-CoV nucleoprotein mAb 1C7C7 (1 µg/mL) was added for 2 hour, followed by HRP-conjugated streptavidin (1:2,000) for 1 hour. OPD substrate was added for 10 minutes, stopped with 3 M HCl, and optical density was measured at 490 nm. The 50% inhibitory dilution (ID_{50}) was calculated using non-linear regression analysis with 100% and 0% constraints.

Pseudotyped virus neutralization assay

Neutralizing antibody titers against WA.1 and BA.3.2 variants were measured using replication-competent vesicular stomatitis virus expressing SARS-CoV-2 spike in place of VSV-G (rcVSV-eGFP-CoV2-S) as previously described [2]. Virus stocks were expended on BHK-ACE2 cells and titrated on Vero-E6 TMPRSS2 cells prior to use. One day before the assay, Vero-E6 TMPRSS2 cells (2×10^5 cells/well) were seeded in 96-well plates. Heat-inactivated sera were initially diluted 1:10 in 1× minimum essential medium (MEM) followed by 3-fold serial dilutions. Diluted sera were incubated with 10,000 $TCID_{50}$ of each VSV-spike pseudotyped virus under conditions identical to those used for live virus microneutralization assays. Following 48-hour incubation, cells were fixed and permeabilized as described above. Fixed cell plates were immunostained with anti-VSV-N monoclonal antibody (10G4, cat. no. EB0009) at a final dilution of 1:3,000 for two hours at room temperature, followed by HRP-conjugated anti-mouse secondary antibody (Rockland, cat. no. 610-1102) at a final dilution of 1:3,000 for 1 hour. OPD substrate was added for 10 minutes, the reaction was stopped with 3 M HCl, and optical density was measured at 490 nm. The ID_{50} titers were calculated as described above.

Antigenic cartography

Antigenic maps were constructed from neutralization data using established multidimensional scaling methods as previously described [3,4]. Neutralizing antibody titers were converted to antigenic distances, where each unit corresponds to a 2-fold difference in neutralization capacity. Variants and sera were positioned in multidimensional space such that Euclidean distances between points accurately reflect antigenic relationships. Maps were optimized to minimize stress between observed and predicted neutralization titers, then projected into two dimensions for visualization. Antigenic cartography maps were generated in R (version 4.3.3) using the Racmacs package (version 1.2.9) [3]. The number of optimization runs was set to 3,000, and the minimum column basis was set to none to allow for maximum flexibility in map construction. The limit of detection (LoD) for neutralizing antibody titers was established at 1:10, and all titers below this threshold were assigned as "<10" in the titer table for subsequent analysis.

Statistical analysis

Statistical analyses were performed using Prism 10 software (GraphPad). Log-transformed neutralization titers, binding AUC values, and binding-to-neutralizing ratios were compared between groups. Normality was assessed using Shapiro-Wilk tests. For non-normally distributed data, Kruskal-Wallis test with Dunn's multiple comparisons test was applied. Wilcoxon matched-pairs signed rank test was used for paired comparisons. Geometric mean titers and geometric mean ratios with 95% confidence intervals were calculated for all analyses. Statistical significance was defined as $p < 0.05$.

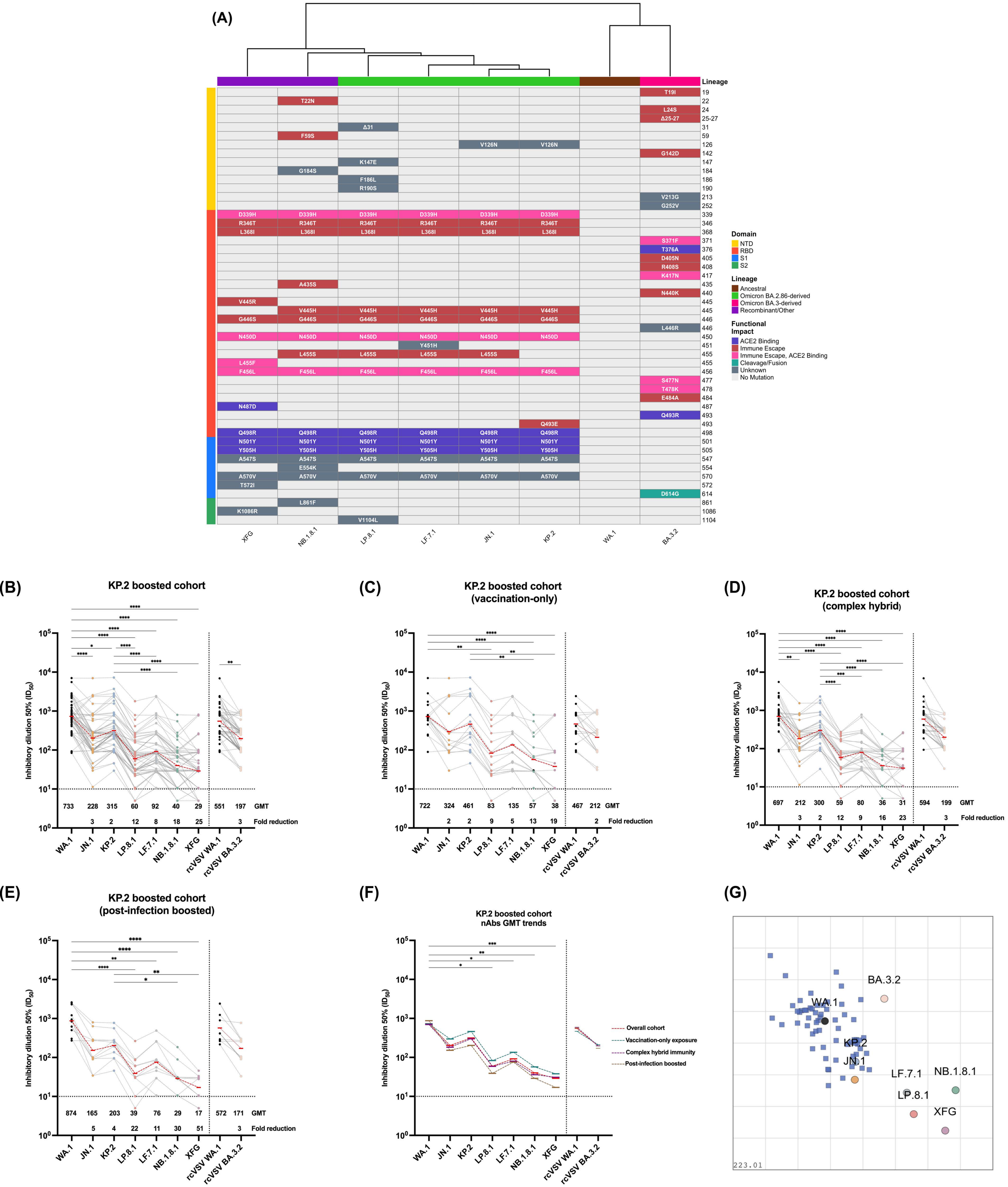
(A)
Lineage
T19I 19
T22N 22
L24S 24
Δ25-27 25-27
Δ31 31
F59S 59
V126N V126N 126
G142D 142
K147E 147
G184S 184
F186L 186
R190S 190
V213G 213
G252V 252
D339H D339H D339H D339H D339H D339H 339
R346T R346T R346T R346T R346T R346T 346
L368I L368I L368I L368I L368I L368I 368
S371F 371
T376A 376
D405N 405
R408S 408
K417N 417
A435S 435
N440K 440
V445R 445
V445H V445H V445H V445H V445H 445
G446S G446S G446S G446S G446S G446S 446
L446R 446
N450D N450D N450D N450D N450D N450D 450
Y451H 451
L455S L455S L455S L455S 455
L455F 455
F456L F456L F456L F456L F456L F456L 456
S477N 477
T478K 478
E484A 484
N487D 487
Q493R 493
Q493E 493
Q498R Q498R Q498R Q498R Q498R Q498R 498
N501Y N501Y N501Y N501Y N501Y N501Y 501
Y505H Y505H Y505H Y505H Y505H Y505H 505
A547S A547S A547S A547S A547S A547S 547
E554K 554
A570V A570V A570V A570V A570V A570V 570
T572I 572
D614G 614
L861F 861
K1086R 1086
V1104L 1104
XFG
NB.1.8.1
LP.8.1
LF.7.1
JN.1
KP.2
WA.1
BA.3.2
Domain
NTD
RBD
S1
S2
Lineage
Ancestral
Omicron BA.2.86-derived
Omicron BA.3-derived
Recombinant/Other
Functional Impact
ACE2 Binding
Immune Escape
Immune Escape, ACE2 Binding
Cleavage/Fusion
Unknown
No Mutation
(B)
KP.2 boosted cohort
Inhibitory dilution 50% (ID50)
733 228 315 60 92 40 29 551 197 GMT
3 2 12 8 18 25 3 Fold reduction
WA.1 JN.1 KP.2 LP.8.1 LF.7.1 NB.1.8.1 XFG rcVSV WA.1 rcVSV BA.3.2
(C)
KP.2 boosted cohort (vaccination-only)
Inhibitory dilution 50% (ID50)
722 324 461 83 135 57 38 467 212 GMT
2 2 9 5 13 19 2 Fold reduction
WA.1 JN.1 KP.2 LP.8.1 LF.7.1 NB.1.8.1 XFG rcVSV WA.1 rcVSV BA.3.2
(D)
KP.2 boosted cohort (complex hybrid)
Inhibitory dilution 50% (ID50)
697 212 300 59 80 36 31 594 199 GMT
3 2 12 9 16 23 3 Fold reduction
WA.1 JN.1 KP.2 LP.8.1 LF.7.1 NB.1.8.1 XFG rcVSV WA.1 rcVSV BA.3.2
(E)
KP.2 boosted cohort (post-infection boosted)
Inhibitory dilution 50% (ID50)
874 165 203 39 76 29 17 572 171 GMT
5 4 22 11 30 51 3 Fold reduction
WA.1 JN.1 KP.2 LP.8.1 LF.7.1 NB.1.8.1 XFG rcVSV WA.1 rcVSV BA.3.2
(F)
KP.2 boosted cohort nAbs GMT trends
Inhibitory dilution 50% (ID50)
Overall cohort
Vaccination-only exposure
Complex hybrid immunity
Post-infection boosted
WA.1 JN.1 KP.2 LP.8.1 LF.7.1 NB.1.8.1 XFG rcVSV WA.1 rcVSV BA.3.2
(G)
BA.3.2
WA.1
KP.2
JN.1
LF.7.1
NB.1.8.1
LP.8.1
XFG
223.01

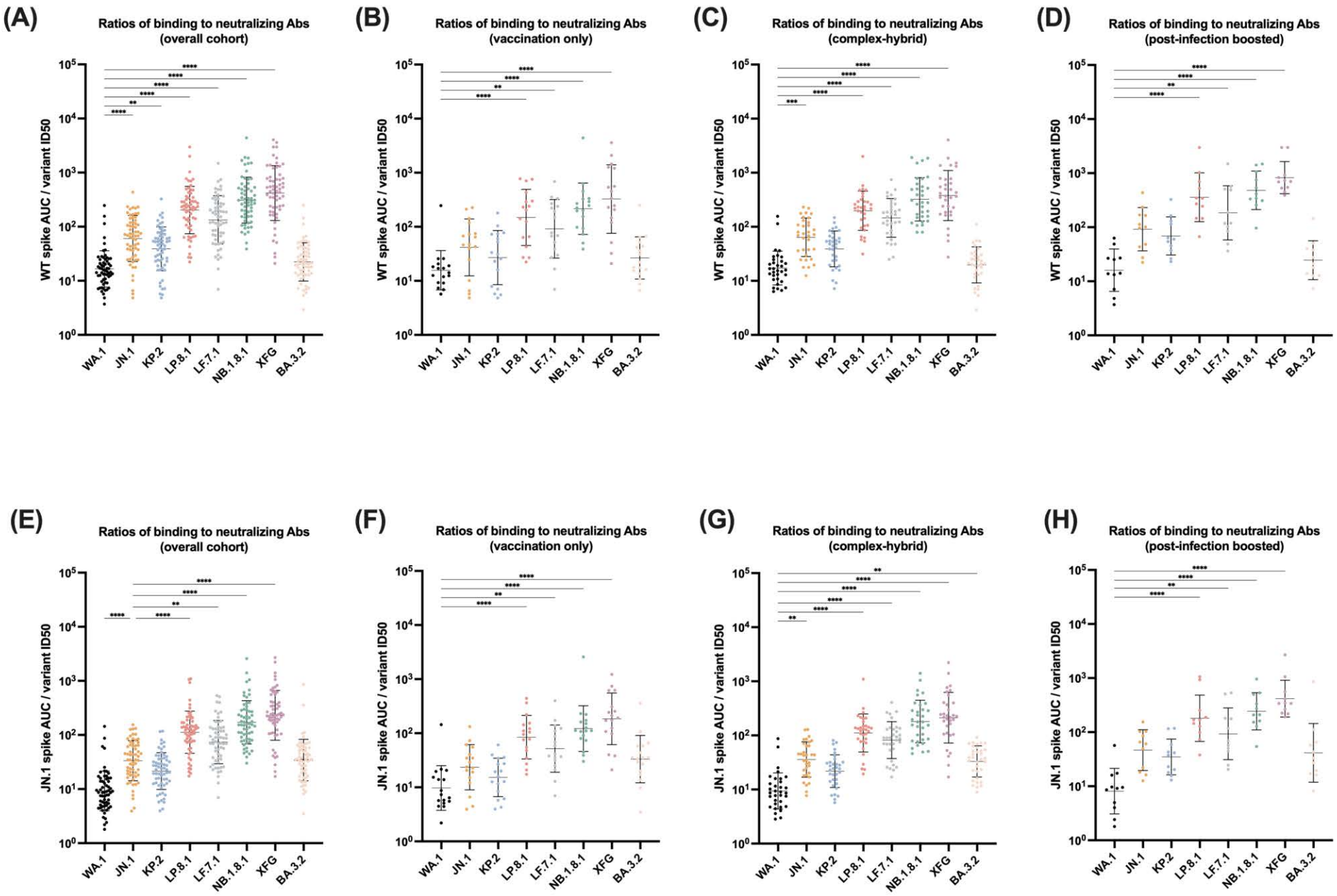
(A)
Ratios of binding to neutralizing Abs
(overall cohort)
WT spike AUC / variant ID50
(B)
Ratios of binding to neutralizing Abs
(vaccination only)
WT spike AUC / variant ID50
(C)
Ratios of binding to neutralizing Abs
(complex-hybrid)
WT spike AUC / variant ID50
(D)
Ratios of binding to neutralizing Abs
(post-infection boosted)
WT spike AUC / variant ID50
(E)
Ratios of binding to neutralizing Abs
(overall cohort)
JN.1 spike AUC / variant ID50
(F)
Ratios of binding to neutralizing Abs
(vaccination only)
JN.1 spike AUC / variant ID50
(G)
Ratios of binding to neutralizing Abs
(complex-hybrid)
JN.1 spike AUC / variant ID50
(H)
Ratios of binding to neutralizing Abs
(post-infection boosted)
JN.1 spike AUC / variant ID50
WA.1
JN.1
KP.2
LP.8.1
LF.7.1
NB.1.8.1
XFG
BA.3.2

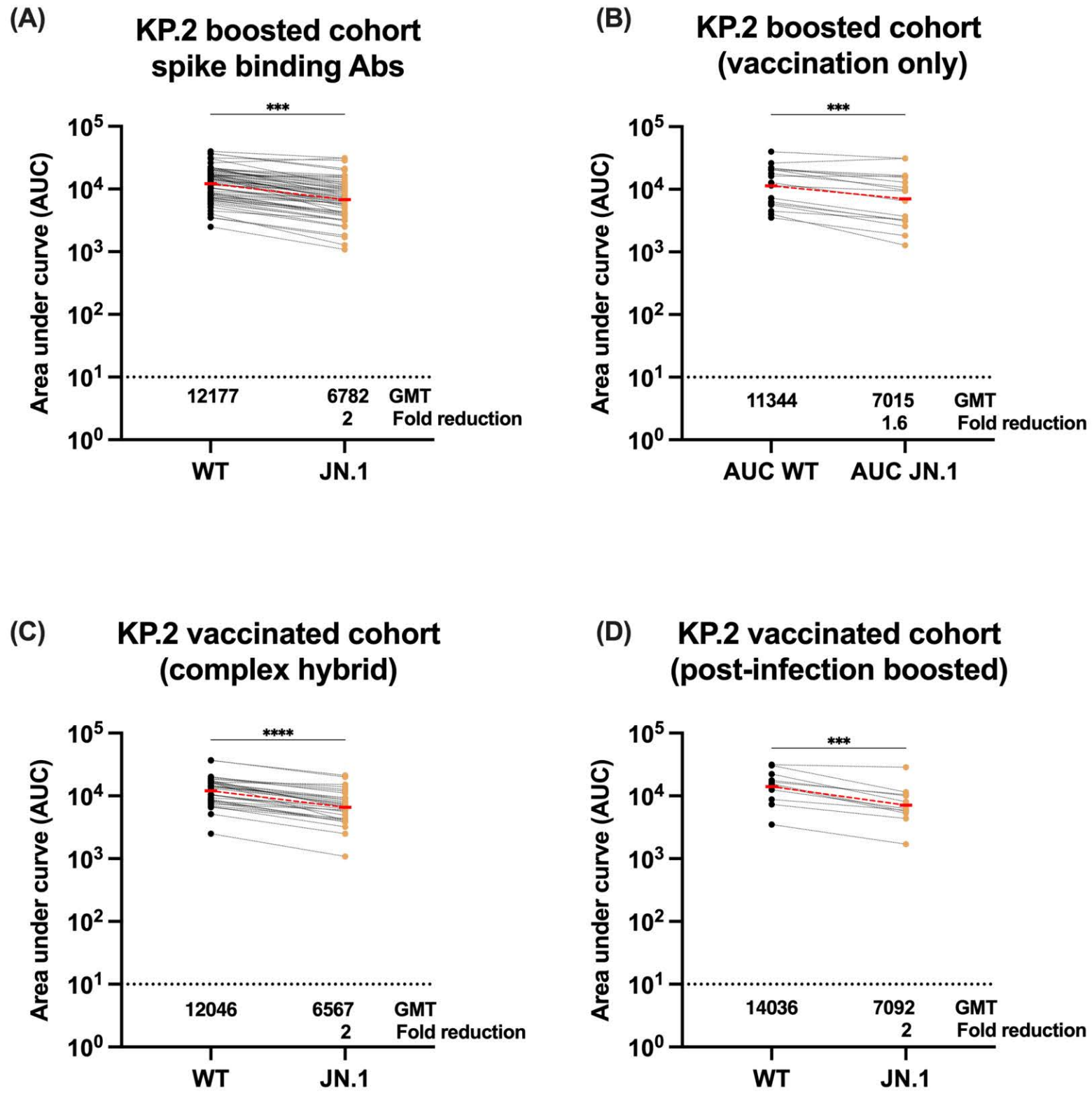
(A)
KP.2 boosted cohort
spike binding Abs
***
Area under curve (AUC)
10^5
10^4
10^3
10^2
10^1
10^0
12177
6782
GMT
2
Fold reduction
WT
JN.1
(B)
KP.2 boosted cohort
(vaccination only)
***
Area under curve (AUC)
11344
7015
GMT
1.6
Fold reduction
AUC WT
AUC JN.1
(C)
KP.2 vaccinated cohort
(complex hybrid)
****
Area under curve (AUC)
12046
6567
GMT
2
Fold reduction
WT
JN.1
(D)
KP.2 vaccinated cohort
(post-infection boosted)
***
Area under curve (AUC)
14036
7092
GMT
2
Fold reduction
WT
JN.1